ResearchGate

See discussions, stats, and author profiles for this publication at: https://www.researchgate.net/publication/263984311

The Kinetics of H2−D2 Exchange over Pd, Cu, and PdCu Surfaces

ARTICLE *in* THE JOURNAL OF PHYSICAL CHEMISTRY C · NOVEMBER 2011

Impact Factor: 4.77 · DOI: 10.1021/jp2076885

CITATIONS
13

READS
32

4 AUTHORS, INCLUDING:

Casey O'Brien
Army Research Laboratory, Adelphi Laborat…
17 PUBLICATIONS **166** CITATIONS
SEE PROFILE

Andrew J. Gellman
Carnegie Mellon University
278 PUBLICATIONS **5,086** CITATIONS
SEE PROFILE

Available from: Casey O'Brien
Retrieved on: 26 January 2016

THE JOURNAL OF PHYSICAL CHEMISTRY C

ARTICLE

pubs.acs.org/JPCC

The Kinetics of H_2-D_2 Exchange over Pd, Cu, and PdCu Surfaces

Casey P. O'Brien,[†,‡] James B. Miller,[†,‡] Bryan D. Morreale,[†] and Andrew J. Gellman*[,†,‡]

[†]National Energy Technology Laboratory, US Department of Energy, P.O. Box 10940, Pittsburgh, Pennsylvania 15236, United States

[‡]Department of Chemical Engineering, Carnegie Mellon University, Pittsburgh, Pennsylvania 15213, United States

ABSTRACT: PdCu alloy membranes are promising candidates for hydrogen separation from H_2S-containing gas mixtures. Dissociative H_2 adsorption and associative desorption are important steps in the process of hydrogen transport across PdCu membranes; however, the kinetics of H_2 adsorption and desorption on PdCu surfaces are not well understood. In this work, the kinetics and energetics of H_2 adsorption and desorption on Pd, Cu, and PdCu surfaces are investigated by microkinetic analysis of H_2-D_2 exchange ($H_2 + D_2 \rightarrow 2HD$) over fixed beds of Pd, Cu, $Pd_{70}Cu_{30}$, and $Pd_{47}Cu_{53}$ foils at near-ambient pressure and temperatures in the range 300−900 K. The rate of H_2-D_2 exchange over Cu, which is the least active H_2-D_2 exchange catalyst used in this study, is limited by the rate of H_2 adsorption due to the large activation barrier to dissociative H_2 adsorption on Cu ($\Delta E_{ads}^{\ddagger} = 0.54 \pm 0.06$ eV). The Cu content of the PdCu alloys and the crystal structures of the Pd-hydride phases (α- and β-PdH) and of $Pd_{47}Cu_{53}$ (body-centered cubic and face-centered cubic (FCC)) all have a significant impact on the kinetics of H_2-D_2 exchange. The activation barriers to dissociative H_2 adsorption, $\Delta E_{ads}^{\ddagger}$, on β-Pd-hydride (0.3 ± 0.1 eV), α-Pd-hydride (0.12 ± 0.04 eV), $Pd_{70}Cu_{30}$ (0.09 ± 0.02 eV), B2 $Pd_{47}Cu_{53}$ (0.15 ± 0.02 eV), and FCC $Pd_{47}Cu_{53}$ (0.00 ± 0.02 eV), are relatively small compared to the adsorption barrier on Cu. Over these surfaces, the rates of H_2-D_2 exchange are limited primarily by the rate of HD desorption. H_2-D_2 exchange activities in the desorption-limited cases decrease (FCC $Pd_{47}Cu_{53}$ > $Pd_{70}Cu_{30}$ > B2 $Pd_{47}Cu_{53}$ > β-PdH > α-PdH) as the barriers to HD desorption, $\Delta E_{des}^{\ddagger}$, increase in the order FCC $Pd_{47}Cu_{53}$ (0.46 ± 0.03 eV) < $Pd_{70}Cu_{30}$ (0.52 ± 0.02 eV) < β-PdH (0.63 ± 0.03 eV) < B2 $Pd_{47}Cu_{53}$ (0.67 ± 0.03 eV) < α-PdH (0.68 ± 0.06 eV). These results are significant because they demonstrate that, although the rate of H_2 adsorption on pure Cu is very low, Pd can be alloyed with as much as ~50 mol % Cu without significantly reducing its activity for dissociative H_2 adsorption.

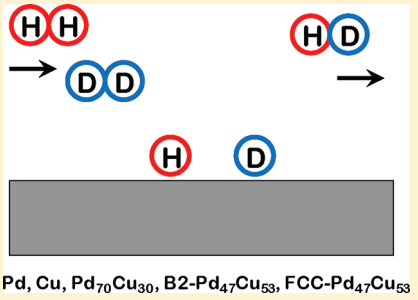

1. INTRODUCTION

Dense Pd membranes are receiving significant attention for hydrogen separation in advanced coal-conversion processes because of their high hydrogen permeability and their near-infinite selectivity.[1,2] However, pure Pd is susceptible to hydrogen embrittlement as a result of the expansion of the Pd lattice during β-Pd-hydride formation.[3,4] Furthermore, H_2S, a coal gasification byproduct, severely inhibits hydrogen permeation through pure Pd.[5−10] PdCu alloys have exhibited resistance to hydrogen embrittlement[11] and improved sulfur tolerance relative to Pd.[6,7,12−15] $Pd_{70}Cu_{30}$ and $Pd_{47}Cu_{53}$ (mol %) are two particularly attractive PdCu alloy compositions because of their sulfur tolerance and because of their relatively high hydrogen permeability.[1,5,7,12,16]

To separate H_2 from mixed gas streams, a Pd-based membrane must dissociatively adsorb H_2 on its upstream surface and associatively desorb H_2 from its downstream surface. The energetics of H_2 dissociation over pure Pd and pure Cu have been well characterized; H_2 dissociates on Pd without significant activation barriers,[17−21] whereas H_2 dissociation on Cu is hindered by a very large activation barrier ($\Delta E_{ads}^{\ddagger} = 0.5-0.7$ eV).[22−32] However, the effect of alloying Pd with Cu on the energetics of the H_2 dissociation reaction is not well understood.

In this work, the energetics of dissociative H_2 adsorption and associative desorption on Pd, Cu, $Pd_{70}Cu_{30}$, and $Pd_{47}Cu_{53}$ foil surfaces have been investigated by microkinetic analysis of H_2-D_2 exchange ($H_2 + D_2 \rightarrow 2HD$) rates measured at near ambient pressure and temperatures in the range 300−900 K. Our results confirm the presence of a large activation barrier to dissociative adsorption of H_2 on the Cu surface, $\Delta E_{ads}^{\ddagger} = 0.54$ eV. In contrast, barriers to H_2 dissociation over Pd, $Pd_{70}Cu_{30}$, and $Pd_{47}Cu_{53}$ are relatively small. We also show that the crystal structures of the Pd phases (β-PdH and α-PdH) and of $Pd_{47}Cu_{53}$ (body-centered cubic (B2) and face-centered cubic (FCC)) have a significant impact on the kinetics of H_2-D_2 exchange. Our results indicate that, although pure Cu has a very low H_2 dissociation activity, Pd can be alloyed with as much as ~50 mol % Cu without significantly reducing H_2 dissociation rates.

2. EXPERIMENTAL SECTION

H_2-D_2 exchange kinetics were measured by flowing H_2, D_2, and Ar through a 4 mm internal diameter quartz tube reactor that was packed with diced foils of Pd, Cu, $Pd_{70}Cu_{30}$, or $Pd_{47}Cu_{53}$. A schematic of the H_2-D_2 exchange reactor is shown in Figure 1. The Pd (Alfa Aesar, 25 μm thick, 99.9% metals purity), Cu (Alfa Aesar, 100 μm thick, 99.95% metals purity), $Pd_{70}Cu_{30}$

Received: August 10, 2011
Revised: October 26, 2011
Published: November 15, 2011

ACS Publications © 2011 American Chemical Society

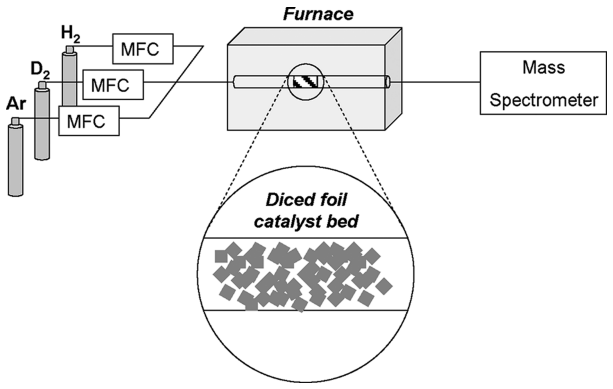

Figure 1. Schematic of the H_2-D_2 exchange reactor. Pd, Cu, $Pd_{70}Cu_{30}$, and $Pd_{47}Cu_{53}$ foil was diced into ~1 mm^2 pieces and packed into a quartz tube reactor placed within a tube furnace. H_2, D_2, and Ar were fed to the reactor while the product gas was analyzed by a mass spectrometer. The flow rates of H_2, D_2, and Ar to the reactor were controlled with mass flow controllers (MFC).

(ACI Alloys, Inc., 100 μm thick, 99.0% metals purity), and $Pd_{47}Cu_{53}$ (ATI Wah Chang, 25 μm thick, 99.0% metals purity) foil were diced into ~1 mm^2 pieces. The total surface area of each catalyst sample was ~19 cm^2. A thermocouple was fixed with a metal wire to the outside of the quartz tube reactor near the catalyst. The reactor was heated in a tube furnace (Barnstead/Thermolyne 211000). Mass flow controllers (Aalborg GFC 17) regulated the flow rates of H_2 (99.999%, Valley National Gases), D_2 (99.999%, Valley National Gases), and Ar (99.999%, Valley National Gases) to the catalyst bed. A ~1 m long, 320 μm internal diameter quartz capillary (Polymicro Technologies) was sealed into the outlet of the quartz tube reactor and the product gas was sampled by a ~15 cm long, 20 μm I.D quartz capillary (Polymicro Technologies) inserted into the outlet of the 320 μm I.D. quartz capillary. The gas samples were analyzed by mass spectrometry (Stanford Research Systems, RGA 200).

All but one of the samples have FCC structures under all conditions of the H_2-D_2 exchange measurements. The $Pd_{47}Cu_{53}$ alloy, however, has a B2 crystal structure at temperatures below ~700 K and a FCC crystal structure at temperatures above ~800 K.[1,6,33] In the temperature range of the H_2-D_2 exchange experiments over the $Pd_{47}Cu_{53}$ alloy (200−500 K), only the B2 crystal structure is thermodynamically stable. However, the FCC phase can also be prepared and kinetically stabilized in this temperature range. Therefore, it was possible to make measurements of H_2-D_2 exchange over both the B2 and FCC phases of the $Pd_{47}Cu_{53}$ alloy. To produce a kinetically stabilized FCC crystal structure, the $Pd_{47}Cu_{53}$ alloy was first annealed in pure H_2 at ~1000 K for ~24 h and then cooled quickly (~15 min) to ~400 K to quench the FCC crystal structure. To produce the B2 structure, the $Pd_{47}Cu_{53}$ alloy was annealed in H_2 at ~700 K for ~48 h. The crystal structures of the B2 and FCC alloy were verified by X-ray diffraction (XRD) following H_2-D_2 exchange experiments; the structures did not change during the H_2-D_2 exchange experiments.

Initially, each catalyst was conditioned in H_2 at ~700 K (~1000 K for Cu and FCC $Pd_{47}Cu_{53}$) for ~24 h. After conditioning, a H_2/D_2/Ar feed gas mixture was introduced to the reactor. Three different feed gas conditions, summarized in Table 1, were used to exercise the kinetic model for H_2-D_2 exchange over a range of total flow rates and partial pressures of

Table 1. Flow Rates of H_2 ($F_{H_2,feed}$), D_2 ($F_{D_2,feed}$), and Ar ($F_{Ar,feed}$) in the Three Different Feed Gas Conditions Used during H_2-D_2 Exchange Experiments and Total Pressure (P_{total}) Measured in the Reactor at Each of the Conditions

feed gas condition	$F_{H_2,feed}$ (mL/min)	$F_{D_2,feed}$ (mL/min)	$F_{Ar,feed}$ (mL/min)	P_{total} (kPa)
$9H_2/9D_2$	9	9	0	121
$4.5H_2/4.5D_2$	4.5	4.5	0	113
$9Ar/4.5H_2/4.5D_2$	4.5	4.5	9	135

H_2 and D_2. The total pressure in the reactor was measured with a Baratron pressure gauge. Starting from the temperature of the conditioning treatment, steady-state H_2, D_2, and HD mass spectrometer signals were collected from the product gas. To minimize the effect of H (or D) evolution from, or absorption into, the bulk of the catalyst on the kinetics of the reaction, the catalyst was cooled in a stepwise manner, and the temperature was stabilized for ~10 min before H_2, D_2, and HD mass spectrometer signals were collected. To show the H evolution from the bulk of the Pd sample during the β-Pd-hydride to α-Pd-hydride phase transition, the experiment was also conducted over the Pd catalyst while heating the sample at a constant rate. To prepare the β-Pd-hydride phase, the Pd catalyst was initially conditioned in H_2 at ~700 K and then cooled in H_2 to ~300 K to saturate the sample with H_2. The H_2/D_2/Ar feed gas was then introduced and the sample was heated at a constant rate of 10 K/min while the product gas composition was analyzed.

The composition of the reactor effluent was calculated assuming that the mass spectrometer signals at $m/q = 2$, 3, and 4 amu obtained from the product gas samples were proportional to the H_2, HD, and D_2 partial pressures between the baseline (0% conversion) and equilibrium conversion. Baseline mass spectrometer signals at m/q = 2, 3, and 4 amu were collected by sampling the feed gases directly without passing them through the catalyst bed. At equilibrium, the H_2/D_2/HD composition in the product gas is given by

$$\frac{P_{HD}^2}{P_{H_2}P_{D_2}} = 4.16\exp\left(\frac{-77.7}{T}\right) \quad (1)$$

where P_{H_2}, P_{D_2}, and P_{HD} are the partial pressures of H_2, D_2, and HD, respectively.[34] The H_2, D_2, and HD partial pressures were then converted into H_2, D_2, and HD flow rates

$$F_i = \frac{F_{total}P_i}{P_{total}} \quad (2)$$

where F_i is the flow rate of each species, F_{total} is the total flow rate, P_i is the partial pressure of each species, and P_{total} is the total pressure. The HD flow rates exiting the catalyst bed during H_2-D_2 exchange experiments were used to determine the temperature dependent rate constants for dissociative adsorption and associative desorption of hydrogen from the surfaces of the various samples.

3. KINETIC MODEL

We made three basic assumptions in deriving the microkinetic model for the H_2-D_2 exchange reaction:

(1) The H_2-D_2 exchange reaction can be modeled by considering only dissociative adsorption and associative desorption of H_2, D_2, and HD under steady state conditions.

(2) Isotopic effects can be ignored (i.e., the adsorption rate constants are the same for H_2, D_2, and HD; and the desorption rate constants are the same for H_2, D_2, and HD).
(3) The activation barriers and pre-exponents in the rate constants for adsorption and desorption are independent of coverage and temperature.

With these three simplifying assumptions, derivation of the H_2-D_2 exchange kinetic model requires substitution of the microkinetic expression for the rate of HD production into an integral mole balance on HD. A detailed derivation of the microkinetic model is given in the Appendix. The flow rate of HD exiting the foil catalyst bed ($F_{HD,out}$) is given by

$$F_{HD,out} = F_{H_2,feed}\left[1 - \exp\left(\frac{-k_{ads}\,p_{total}\,A}{F_{total}\left(1 + \sqrt{2\frac{k_{ads}}{k_{des}}P_{H_2,feed}}\right)^2}\right)\right] \quad (3)$$

where $F_{H_2,feed}$ is the flow rate of H_2 in the feed gas, k_{ads} is the adsorption rate constant, P_{total} is the total pressure in the reactor, A is the catalyst surface area, F_{total} is the total gas flow rate through the reactor, k_{des} is the desorption rate constant, and $P_{H_2,feed}$ is the partial pressure of H_2 in the feed gas. The adsorption rate constant, k_{ads}, and the desorption rate constant, k_{des}, have Arrhenius forms

$$k_{ads} = \upsilon_{ads}\exp\left(\frac{-\Delta E_{ads}^{\ddagger}}{k_B T}\right) \quad (4a)$$

$$k_{des} = \upsilon_{des}\exp\left(\frac{-\Delta E_{des}^{\ddagger}}{k_B T}\right) \quad (4b)$$

where ν_{ads} is the adsorption pre-exponent, $\Delta E_{ads}{}^{\ddagger}$ is the adsorption activation barrier, ν_{des} is the desorption pre-exponent, $\Delta E_{des}{}^{\ddagger}$ is the desorption activation barrier, k_B is the Boltzmann constant, and T is the temperature. The total coverage of H and D atoms during H_2-D_2 exchange is given by

$$\theta = \frac{\sqrt{2\frac{k_{ads}}{k_{des}}P_{H_2,feed}}}{1 + \sqrt{2\frac{k_{ads}}{k_{des}}P_{H_2,feed}}} \quad (5)$$

For each experiment, the partial pressures of H_2 and D_2 were equal; thus the coverages of H and D can be assumed to be equal. Equation 5 implies that the coverage of H and D atoms is constant along the length of the catalyst bed.

To determine the values of ν_{ads}, $\Delta E_{ads}{}^{\ddagger}$, ν_{des}, and $\Delta E_{des}{}^{\ddagger}$ that describe H_2 adsorption and desorption on each surface, a numerical solver was used to find the values of $\log(\nu_{ads})$, $\Delta E_{ads}{}^{\ddagger}$, $\log(\nu_{des})$, and $\Delta E_{des}{}^{\ddagger}$ that minimize the error between the measured HD flow rates and the flow rates predicted by the model over a wide temperature range. The uncertainty in these solver-optimized parameters was estimated with a "SolverAid" program.[35]

4. RESULTS AND DISCUSSION

4.1. H_2-D_2 Exchange over Pd. H_2-D_2 exchange over Pd was carried out by feeding H_2, D_2, and Ar to a Pd foil catalyst bed, with the product gas composition monitored by a mass spectrometer. Mass spectrometer signals were converted to flow rates. Figure 2a shows the HD flow rates exiting the Pd catalyst bed for the three different feed gas conditions: 9 mL/min each of H_2 and D_2, 4.5 mL/min each of H_2 and D_2, and 4.5 mL/min each of H_2 and D_2 diluted with 9 mL/min of Ar. The HD flow rates for the three feed conditions are shown as discrete data points while the fits of the microkinetic model are illustrated with the solid lines. The conversion of H_2 and D_2 into HD increases from 0% at 300 K to reach equilibrium conversion at 550 K.

There is a discontinuity in the HD flow rate exiting the Pd foil catalyst bed at ~410 K for both of the H_2/D_2 feed gas flow rates and at ~400 K for the $Ar/H_2/D_2$ feed gas. The discontinuity in the HD flow occurs at a temperature near that of the β-Pd-hydride to α-Pd-hydride phase transition in a H_2 partial pressure of ~1 atm.[36,37] The temperature of the β-Pd-hydride to α-Pd-hydride phase transition decreases with decreasing H_2 partial pressure, which is consistent with the observation that the discontinuity in the HD flow rate in Figure 2a occurs at a lower temperature for the $Ar/H_2/D_2$ feed gas than for the H_2/D_2 feed gases. These observations suggest that the discontinuity in the HD flow rate exiting the Pd foil catalyst bed is due to the β-Pd-hydride to α-Pd-hydride phase transition; the α-Pd-hydride phase exhibits a lower H_2-D_2 exchange activity than the β-Pd-hydride phase.

It is worth noting that each data point in Figure 2a was collected at constant temperature; the sample was held at each temperature for ~10 min to obtain steady state measurements. A much different result is obtained when the H_2-D_2 exchange experiment is performed over Pd while increasing the reaction temperature at a constant rate. Figure 3 shows the partial pressures of H_2, D_2, HD, and Ar in the product gas during H_2-D_2 exchange over the Pd foil catalyst bed while the catalyst temperature was increased at a constant rate of 10 K/min, with feed gas flow rates of 9 mL/min of Ar and 4.5 mL/min each of H_2 and D_2. Note that, as a result of cooling from 700 K in 1 atm of H_2, the bulk of the Pd was initially saturated in H and in the β-Pd-hydride phase. Because Ar is inert, one would expect the Ar partial pressure in the product gas to remain constant over the course of the experiment. Instead, there is a dip in the Ar partial pressure in the temperature range 420−460 K. Over that same temperature range, there is a spike in the H_2 and HD partial pressures and a dip in the D_2 partial pressure. We believe that H_2 evolution from the Pd bulk during the β-Pd-hydride to α-Pd-hydride phase transition is responsible for the spike in the H_2 partial pressure and the dip in the Ar partial pressure. The β-Pd-hydride phase has a much higher concentration of H atoms in its bulk (H:Pd ≈ 0.6) than the α-Pd-hydride phase (H:Pd ≈ 0.03),[38] and therefore, a large amount of hydrogen must evolve from the Pd bulk during the β-Pd-hydride to α-Pd-hydride phase transition. The temperature of the discontinuity in the steady-state HD flow rate exiting the Pd foil catalyst bed (~400 K) is not exactly the same as the temperature of the spike in the H_2 partial pressure (420−460 K) observed while the Pd catalyst temperature was increased at a constant rate. This is likely because the β-Pd-hydride to α-Pd-hydride phase transition does not occur instantaneously.

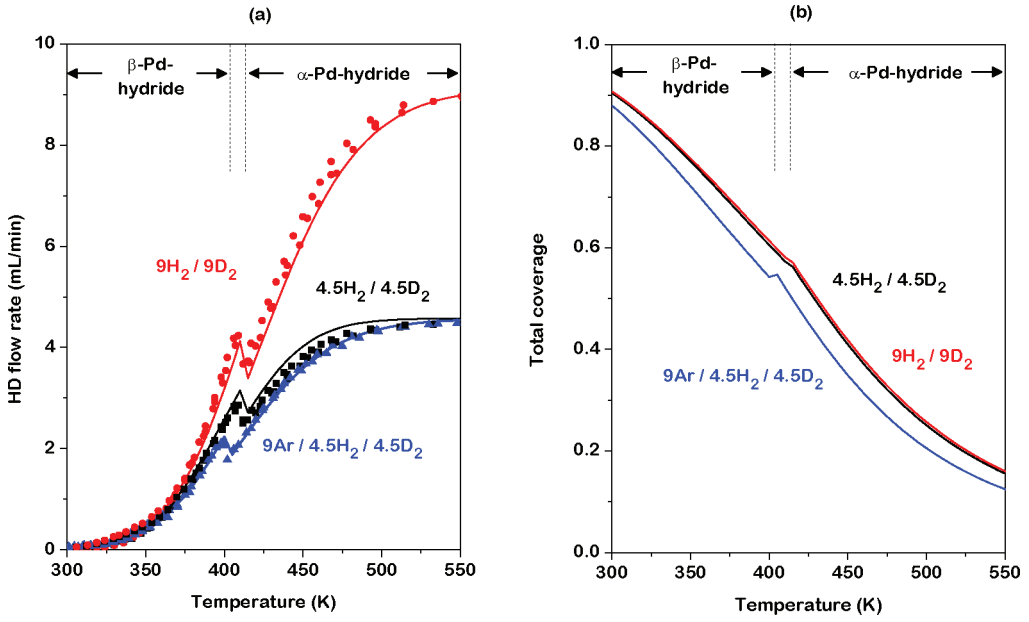

Figure 2. (a) Experimental (points) and modeled (lines) HD flow rates vs temperature exiting a ~19 cm^2 Pd foil catalyst bed for three different feed gas conditions (shown in units of mL/min). The discontinuity in the HD flow rate is due to a phase change from β-Pd-hydride to α-Pd-hydride. Modeled HD flow rates were calculated using the H_2-D_2 exchange model, eq 3, and the solver-optimized values for ν_{ads}, $\Delta E_{ads}^{\ddagger}$, ν_{des}, $\Delta E_{des}^{\ddagger}$. (b) Total coverage of H and D atoms during H_2-D_2 exchange over the Pd foil catalyst bed. The coverage was calculated using eq 5 and the solver-optimized values for ν_{ads}, $\Delta E_{ads}^{\ddagger}$, ν_{des}, $\Delta E_{des}^{\ddagger}$.

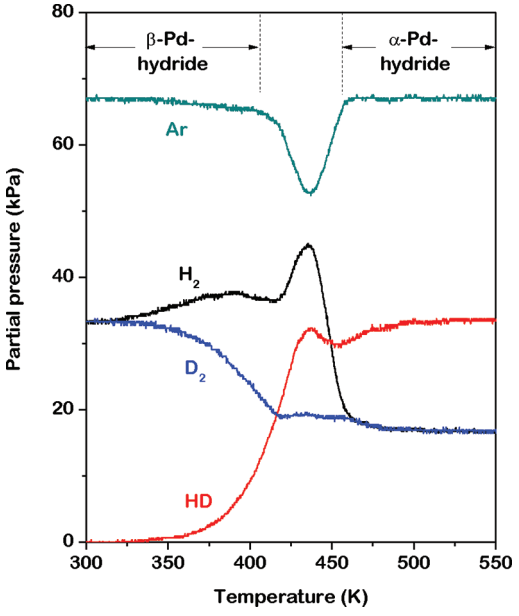

Figure 3. Partial pressures of H_2, D_2, HD, and Ar in the product gas during H_2-D_2 exchange over a Pd foil catalyst with feed gas flow rates of 9 mL/min of Ar and 4.5 mL/min each of H_2 and D_2 and while heating the catalyst at 10 K/min. The spike in the H_2 partial pressure in the temperature range ~420 and ~460 K, and the dip in the Ar partial pressure in the same temperature range, is due to hydrogen evolution from the bulk of Pd during the β-Pd-hydride to α-Pd-hydride phase transition. The higher solubility of H in Pd than that of D in Pd could explain why no spike was observed in the D_2 partial pressure.

To determine the parameters that describe H_2 adsorption (ν_{ads} and $\Delta E_{ads}^{\ddagger}$) and H_2 desorption (ν_{des} and $\Delta E_{des}^{\ddagger}$) on β-Pd-hydride and α-Pd-hydride, a numerical solver was used to find the values of $\log(\nu_{ads})$, $\Delta E_{ads}^{\ddagger}$, $\log(\nu_{des})$, and $\Delta E_{des}^{\ddagger}$ that minimize the error between the modeled and the measured HD flow rates over the experimental temperature range. We modeled H_2-D_2 exchange over β-Pd-hydride and α-Pd-hydride separately. The solver-optimized values for the parameters associated with the α- and β-Pd-hydride phases are summarized in Table 2.

By use of the solver-optimized values for ν_{ads}, $\Delta E_{ads}^{\ddagger}$, ν_{des}, and $\Delta E_{des}^{\ddagger}$ associated with the β-Pd-hydride phases, HD flow rates were calculated with the H_2-D_2 exchange model, eq 3, at temperatures <410 K (<400 K for the $9Ar/4.5H_2/4.5D_2$ feed gas). At temperatures >410 K (>400 K for the $9Ar/4.5H_2/4.5D_2$ feed gas), HD flow rates were calculated using the solver-optimized parameters associated with the α-Pd-hydride phase. Figure 2a shows that the modeled HD flow rates (solid lines) fit the experimental HD flow rates reasonably well for both the β-Pd-hydride and α-Pd-hydride phases and across the entire temperature range of the experiment (300−550 K).

The total coverage of H and D atoms during H_2-D_2 exchange over Pd was calculated using eq 5 and the solver-optimized values of ν_{ads}, $\Delta E_{ads}^{\ddagger}$, ν_{des}, found for the β-Pd-hydride phase at temperatures <410 K (<400 K for the $9Ar/4.5H_2/4.5D_2$ feed gas) and those for the α-Pd-hydride at temperatures >410 K (>400 K for the $9Ar/4.5H_2/4.5D_2$). Figure 2b shows the total coverage of H and D atoms on the Pd surface during H_2-D_2 exchange with the three different feed gas conditions and for the temperature range 300−550 K. At low temperature (~300 K), the β-Pd-hydride surface is nearly saturated with H and D atoms. As the temperature increases, the total coverage decreases for all three feed gas conditions. Diluting the H_2/D_2 feed gas with Ar ($9Ar/4.5H_2/4.5D_2$), which reduces the rate of H_2 and D_2 adsorption by lowering the H_2 and D_2 partial pressures, reduces the total coverage of H and D atoms. At ~410 K (400 K for the $9Ar/4.5H_2/4.5D_2$), there is a discontinuity in the total coverage due to the β-Pd-hydride to α-Pd-hydride phase transition. As the

Table 2. Summary of the Adsorption Pre-Exponents (ν_{ads}), Adsorption Barriers ($\Delta E_{ads}^{\ddagger}$), Desorption Pre-Exponents (ν_{des}), Desorption Barriers ($\Delta E_{des}^{\ddagger}$), and Energies of Adsorption of H_2 (ΔE_{ads}) on β-Pd-hydride, α-Pd-hydride, Cu, $Pd_{70}Cu_{30}$, B2 $Pd_{47}Cu_{53}$, and FCC $Pd_{47}Cu_{53}$

	log ν_{ads} (mol/m^2/s/Pa)	$\Delta E_{ads}^{\ddagger}$ (eV)	log ν_{des} (mol/m^2/s)	$\Delta E_{des}^{\ddagger}$ (eV)	ΔE_{ads} (eV)
β-Pd-hydride	-3.7 ± 0.7	0.3 ± 0.1	5.8 ± 0.4	0.63 ± 0.03	-0.3 ± 0.1
α-Pd-hydride	-5.4 ± 0.4	0.12 ± 0.04	6.3 ± 0.8	0.68 ± 0.06	-0.56 ± 0.07
Cu	-3.4 ± 0.5	0.54 ± 0.06	4 ± 5	0.6 ± 0.7	0.0 ± 0.7
$Pd_{70}Cu_{30}$	-5.6 ± 0.2	0.09 ± 0.02	5.7 ± 0.3	0.52 ± 0.02	-0.43 ± 0.03
B2 $Pd_{47}Cu_{53}$	-5.2 ± 0.2	0.15 ± 0.02	7.4 ± 0.5	0.67 ± 0.03	-0.52 ± 0.04
FCC $Pd_{47}Cu_{53}$	-6.6 ± 0.2	0.00 ± 0.02	6.5 ± 0.5	0.46 ± 0.03	-0.46 ± 0.03

temperature increases further, the total coverage continues to decrease.

The discontinuity in the HD flow rate exiting the Pd foil catalyst bed (Figure 2a) clearly indicates that there is a difference in the energetics of H_2 adsorption/desorption on the β-Pd-hydride and α-Pd-hydride surfaces. There is a significantly larger barrier to H_2 adsorption ($\Delta E_{ads}^{\ddagger} = 0.3 \pm 0.1$ eV) on the β-Pd-hydride surface than on the α-Pd-hydride surface ($\Delta E_{ads}^{\ddagger} = 0.12 \pm 0.04$ eV). The heat of adsorption ($\Delta E_{ads} = \Delta E_{ads}^{\ddagger} - \Delta E_{des}^{\ddagger}$) of H_2 on the β-Pd-hydride surface ($\Delta E_{ads} = -0.3 \pm 0.1$ eV) is significantly less negative than that on the α-Pd-hydride surface ($\Delta E_{ads} = -0.56 \pm 0.07$ eV), indicating that H atoms are less stable on the β-Pd-hydride surface than on the α-Pd-hydride surface. The activation barrier to H_2 desorption from β-Pd-hydride ($\Delta E_{des}^{\ddagger} = 0.63 \pm 0.03$ eV) is not significantly different than that from α-Pd-hydride ($\Delta E_{des}^{\ddagger} = 0.68 \pm 0.06$).

There are two differences between the β-Pd-hydride and α-Pd-hydride phases that might explain the difference between the heats of adsorption of H_2 on the two phases. First, the lattice constant of β-Pd-hydride ($\sim$4.02 Å) is significantly larger than the lattice constant of α-Pd-hydride ($\sim$3.89 Å).[39] However, expansion of the Pd lattice has been shown to *increase* the stability of adsorbed hydrogen,[40] which is inconsistent with our observation that H atoms are more stable on the surface of the α-Pd-hydride which has the small lattice constant. Second, the concentration of H atoms in the bulk of β-Pd-hydride (H:Pd $\approx$ 0.6) is considerably higher than that in the bulk of α-Pd-hydride (H:Pd $\approx$ 0.03).[37] Sykes et al.[41] have recently reported that H atoms in the Pd(111) subsurface destabilize H atoms at top-surface sites directly above the them. These results are consistent with our observation that α-Pd-hydride, with a smaller concentration of subsurface H atoms than β-Pd-hydride, stabilizes adsorbed H-atoms more effectively.

There have been many experimental[17,18,36,42−44] and theoretical[36,45−47] studies of H_2 adsorption and desorption on Pd surfaces, most done with Pd single crystals in ultrahigh vacuum. Comparison of these studies to our work is not straightforward because we use a polycrystalline Pd foil, which probably forms Pd-hydride phases at near-ambient pressures. There have been few studies of H_2 adsorption and desorption on polycrystalline Pd-hydride surfaces at near-ambient pressure.[36,42,44] In one study,[36] the activation barriers to H_2 desorption from β-Pd-hydride and α-Pd-hydride were determined from kinetic analysis of H_2-D_2 exchange over a thin Pd film at near-ambient pressures. Those authors reported activation barriers for H_2 desorption from β-Pd-hydride ($\Delta E_{des}^{\ddagger} = 0.33$ eV) and α-Pd-hydride ($\Delta E_{des}^{\ddagger} = 0.27$ eV) that were much lower than the values obtained in this work ($\Delta E_{des}^{\ddagger} = 0.63 \pm 0.03$ eV on β-Pd-hydride and $\Delta E_{des}^{\ddagger} = 0.68 \pm 0.06$ on α-Pd-hydride). However, in their calculation of the desorption barrier, they assumed that the surface was saturated with H, which we show (Figure 2b) not to be the case.

In summary, there is a discontinuity in the rate of H_2-D_2 exchange over the Pd foil catalyst bed at a temperature of $\sim$400 K that is related to the β-Pd-hydride to α-Pd-hydride phase transition. Microkinetic analysis of the H_2-D_2 exchange reaction indicates that the energetics of H_2 adsorption on β-Pd-hydride is significantly different than on α-Pd-hydride. The activation barrier to H_2 adsorption on the β-Pd-hydride surface ($\Delta E_{ads}^{\ddagger} = 0.3 \pm 0.1$ eV) is significantly higher than that on the α-Pd-hydride surface ($\Delta E_{ads}^{\ddagger} = 0.12 \pm 0.04$ eV), and the heat of adsorption of H_2 on the β-Pd-hydride surface ($\Delta E_{ads}^{\ddagger} = -0.3 \pm 0.1$ eV) is significantly less negative than that on the α-Pd-hydride surface ($\Delta E_{ads}^{\ddagger} = -0.56 \pm 0.07$ eV). These differences are likely related to differences in subsurface H atom concentrations in the two phases.

4.2. H_2-D_2 Exchange over Cu. H_2-D_2 exchange over Cu was carried out using a methodology similar to that used for Pd. Figure 4a shows the HD flow rates exiting the Cu foil catalyst bed with the three different feed gas conditions: 9 mL/min each of H_2 and D_2, 4.5 mL/min each of H_2 and D_2, and 4.5 mL/min each of H_2 and D_2 diluted with 9 mL/min of Ar. In contrast to Pd, there are no discontinuities in the HD flow rate exiting the Cu foil catalyst bed, and there was no evidence of Cu-hydride formation. Note also that the temperature range over which one observes significant conversion is much higher than over Pd, indicating that Cu is much less active for H_2-D_2 exchange than Pd.

The solver-optimized parameters for H_2-D_2 exchange over Cu were as follows: $\nu_{ads} = 10^{-3.4\pm0.5}$ mol/m^2/s/Pa, $\Delta E_{ads}^{\ddagger} = 0.54 \pm 0.06$ eV, $\nu_{des} = 10^{4\pm5}$ mol/m^2/s, and $\Delta E_{des}^{\ddagger} = 0.6 \pm 0.7$ eV. The large uncertainties in the desorption pre-exponent ($10^{4\pm5}$ mol/m^2/s) and desorption barrier (0.6 ± 0.7 eV) indicate that the rate of H_2-D_2 exchange is insensitive to the parameters associated with H_2 desorption and, therefore, that the rate of H_2-D_2 exchange over Cu is limited by the rate of H_2 adsorption. HD flow rates exiting the Cu foil catalyst were calculated with the H_2-D_2 exchange model, eq 3, and the solver-optimized values for ν_{ads}, $\Delta E_{ads}^{\ddagger}$, ν_{des}, and $\Delta E_{des}^{\ddagger}$; Figure 4a shows that the model (solid lines) fits the experimental data very well. Because the rate of H_2-D_2 exchange over Cu is limited by the rate of H_2 and D_2 adsorption, which depends on the H_2 and D_2 partial pressures, diluting the $4.5H_2/4.5D_2$ feed gas with Ar ($9Ar/4.5H_2/4.5D_2$) significantly reduces the HD flow rate exiting the Cu foil catalyst bed. Dilution induced suppression of exchange activity was observed experimentally and was accurately predicted by the model.

The total coverage of H and D atoms during H_2-D_2 exchange over Cu was calculated with eq 5 and is plotted in Figure 4b.

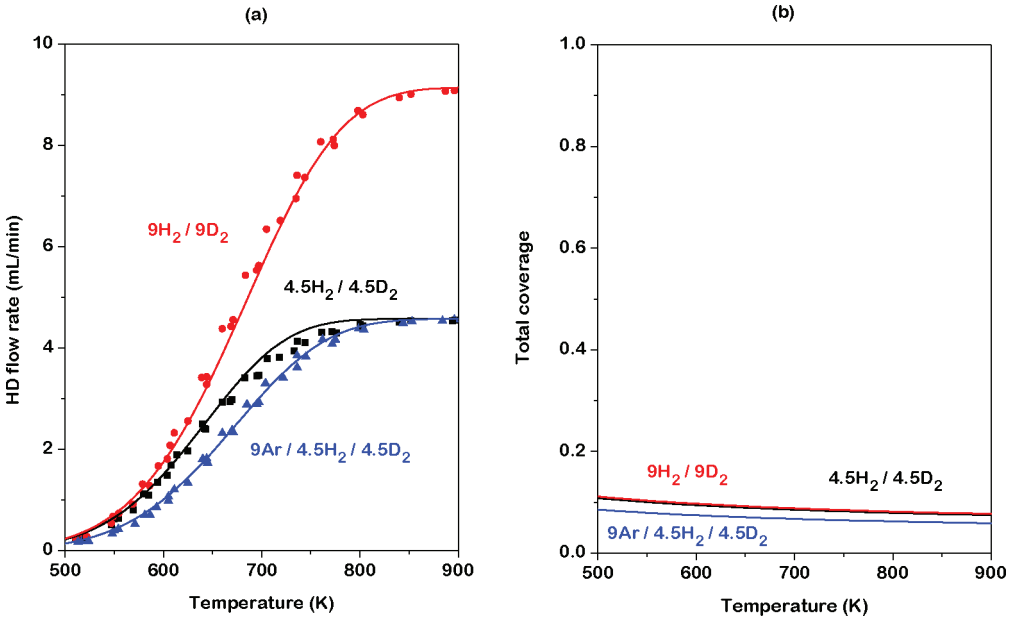

Figure 4. (a) Experimental (points) and modeled (lines) HD flow rates versus temperature exiting a Cu foil catalyst bed for three different feed gas conditions (shown in units of mL/min). Modeled HD flow rates were calculated with eq 3 and the solver-optimized values for ν_{ads}, $\Delta E_{ads}^{\ddagger}$, ν_{des}, $\Delta E_{des}^{\ddagger}$. (b) Total coverage of H and D atoms during H_2-D_2 exchange over the Cu foil catalyst bed. The total coverage was calculated using eq 5 and the solver-optimized values for ν_{ads}, $\Delta E_{ads}^{\ddagger}$, ν_{des}, $\Delta E_{des}^{\ddagger}$.

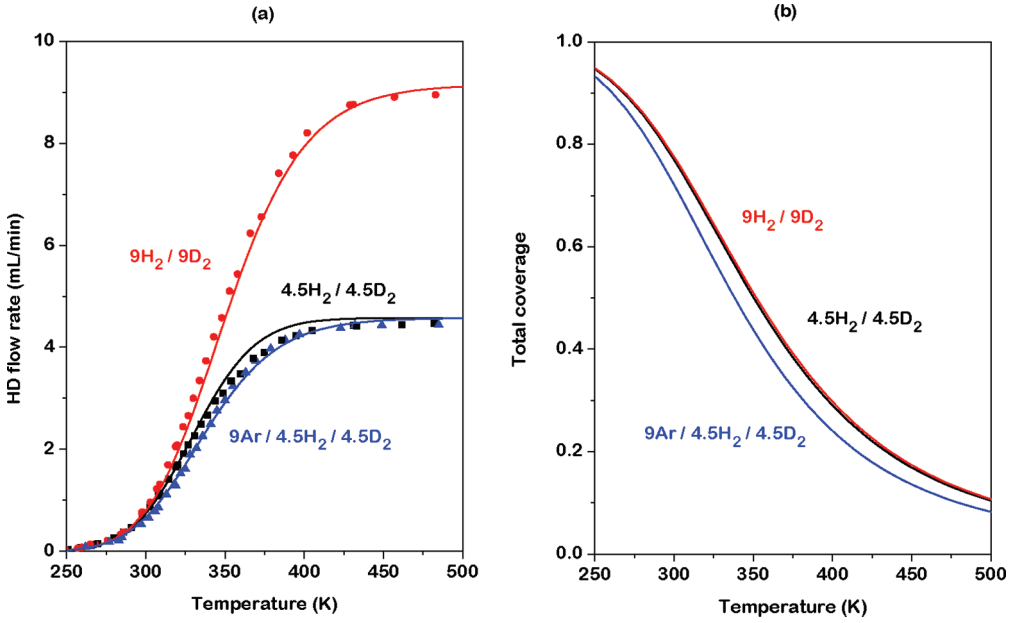

Figure 5. (a) Experimental (points) and modeled (lines) HD flow rates versus temperature exiting a $Pd_{70}Cu_{30}$ foil catalyst bed for three different feed gas conditions (shown in units of mL/min). Modeled HD flow rates were calculated using the H_2-D_2 exchange model, eq 3, and the solver-optimized values for ν_{ads}, $\Delta E_{ads}^{\ddagger}$, ν_{des}, $\Delta E_{des}^{\ddagger}$. (b) Total coverage of H and D atoms during H_2-D_2 exchange over the $Pd_{70}Cu_{30}$ foil catalyst bed, calculated using eq 5 and the solver-optimized values for ν_{ads}, $\Delta E_{ads}^{\ddagger}$, ν_{des}, $\Delta E_{des}^{\ddagger}$.

In contrast to the coverage of H and D atoms on Pd during H_2-D_2 exchange (Figure 2b), the coverage of H and D atoms on the Cu surface is nearly constant throughout the temperature range of the H_2-D_2 exchange reaction and is about one-tenth the saturation coverage. The coverage of H and D atoms is low because the activation barrier to H_2 adsorption on Cu is high ($\Delta E_{ads}^{\ddagger} = 0.54 \pm 0.06$ eV), and as a result, the rate of adsorption is low.

The energetics of H_2 adsorption and desorption on Cu has been well characterized experimentally[24,25,27−29] and theoretically[22,23,26,30,32] in the literature. Most of the reported values for the H_2 adsorption barrier on Cu single crystals are in the range $\Delta E_{ads}^{\ddagger} = 0.5$ to 0.7 eV.[23−32] Our analysis indicates that the activation barrier to H_2 adsorption on polycrystalline Cu foil is $\Delta E_{ads}^{\ddagger} = 0.54 \pm 0.06$ eV, which is in good agreement with the literature. Although the value obtained from this work for the

dx.doi.org/10.1021/jp2076885 |J. Phys. Chem. C 2011, 115, 24221–24230

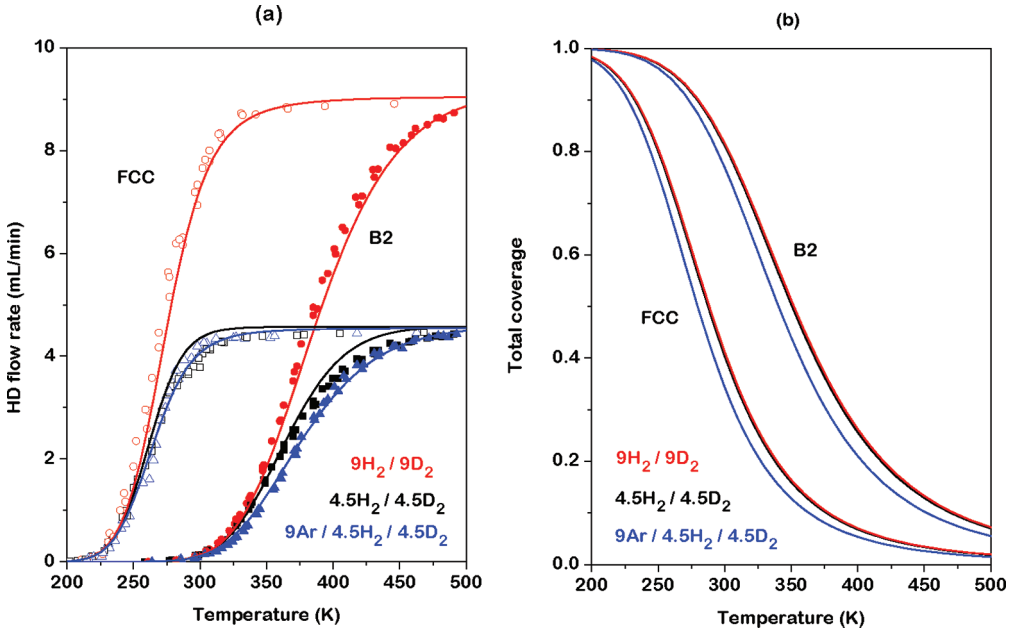

Figure 6. (a) Experimental (points) and modeled (lines) HD flow rates versus temperature exiting a $Pd_{47}Cu_{53}$ foil catalyst bed with a B2 crystal structure and with a FCC crystal structure. Modeled HD flow rates were calculated using the H_2-D_2 exchange model, eq 3, and the solver-optimized values for ν_{ads}, $\Delta E_{ads}^{\ddagger}$, ν_{des}, $\Delta E_{des}^{\ddagger}$. (b) Total coverage of H and D atoms during H_2-D_2 exchange over the B2 and FCC $Pd_{47}Cu_{53}$ foil catalyst beds. The coverage was calculated using eq 5 and the solver-optimized values for ν_{ads}, $\Delta E_{ads}^{\ddagger}$, ν_{des}, $\Delta E_{des}^{\ddagger}$.

H_2 desorption barrier on Cu ($\Delta E_{des}^{\ddagger} = 0.6 \pm 0.7$ eV) has a large uncertainty, Campbell and Campbell[27] reported a barrier to H_2 desorption on Cu(110) of $\Delta E_{des}^{\ddagger} = 0.57$ eV, which is similar to our mean value.

4.3. H_2-D_2 Exchange over $Pd_{70}Cu_{30}$. The energetics of H_2 dissociation over $Pd_{70}Cu_{30}$ have been investigated by microkinetic analysis of H_2-D_2 exchange data obtained over a $Pd_{70}Cu_{30}$ foil catalyst bed. Figure 5a shows the HD flow rates exiting a $Pd_{70}Cu_{30}$ foil catalyst bed with the three different feed gas conditions. There are no discontinuities in the HD flow rate exiting the $Pd_{70}Cu_{30}$ foil catalyst bed, and therefore, there was no evidence of bulk hydride formation. The solver-optimized values of the parameters that describe H_2-D_2 exchange over $Pd_{70}Cu_{30}$ are listed in Table 2. To the best of our knowledge, these are the first reported experimental measurements of the activation barriers to H_2 adsorption and desorption on the $Pd_{70}Cu_{30}$ surface. Using the mean values of these solver-optimized parameters, the predicted HD flow rates were calculated with the H_2-D_2 exchange model, eq 3. A comparison of the modeled and experimental HD flow rates is shown in Figure 5a; the model fits the experimental data very well.

The total coverage of H and D atoms during H_2-D_2 exchange over $Pd_{70}Cu_{30}$ was calculated using eq 5 and the solver-optimized values for ν_{ads}, $\Delta E_{des}^{\ddagger}$, ν_{des}, and $\Delta E_{ads}^{\ddagger}$. Figure 5b shows the total coverage of H and D atoms during H_2-D_2 exchange over $Pd_{70}Cu_{30}$ with the three different feed gas conditions. The evolution of the total coverage on the $Pd_{70}Cu_{30}$ surface with increasing temperature resembles that of Pd (Figure 2) more closely than QJ;it does that of Cu (Figure 4). At low temperature (~250 K), the $Pd_{70}Cu_{30}$ surface is nearly saturated with H and D atoms. As the temperature increases, the total coverage decreases. Diluting the feed gas with Ar reduces the rate of adsorption and reduces the total coverage of H and D atoms.

Diluting the H_2/D_2 feed gas with Ar did not, however, significantly reduce the rate of HD formation over the $Pd_{70}Cu_{30}$ foil catalyst bed (Figure 5a). This indicates that the rate of H_2-D_2 exchange over the $Pd_{70}Cu_{30}$ foil catalyst was controlled by the rate of H_2 desorption, which is independent of the H_2 and D_2 partial pressures, rather than by the rate of H_2 adsorption. As a result, there was a relatively high coverage of H and D atoms during H_2-D_2 exchange over $Pd_{70}Cu_{30}$ (Figure 5b). Microkinetic analysis of H_2-D_2 exchange over $Pd_{70}Cu_{30}$ confirms desorption limited exchange: the barrier to H_2 adsorption on $Pd_{70}Cu_{30}$ ($\Delta E_{ads}^{\ddagger} = 0.09 \pm 0.02$ eV) is small relative to the barrier to H_2 desorption on $Pd_{70}Cu_{30}$ ($\Delta E_{des}^{\ddagger} = 0.52 \pm 0.02$ eV).

4.4. H_2-D_2 Exchange over $Pd_{47}Cu_{53}$. H_2-D_2 exchange was performed over both the B2 and FCC phases of the $Pd_{47}Cu_{53}$ alloy. The procedure for preparing the B2 and FCC phases is given in section 2. Figure 6a shows the HD flow rates exiting the B2 and FCC $Pd_{47}Cu_{53}$ foil catalyst beds with three different feed gas conditions. The FCC crystal structure of the $Pd_{47}Cu_{53}$ alloy is significantly more active for H_2-D_2 exchange than the B2 crystal structure. The solver-optimized values of the parameters that describe H_2-D_2 exchange over B2 and FCC $Pd_{47}Cu_{53}$ are summarized in Table 2. To our knowledge, these are the first reported measurements of the barriers to H_2 adsorption and desorption on B2 or FCC $Pd_{47}Cu_{53}$ surfaces. By use of the solver-optimized parameters, HD flow rates were calculated for the B2 and FCC phases of $Pd_{47}Cu_{53}$ with the three different feed gas conditions. Figure 6a shows that the model fits the experimental data reasonably well.

The total coverages of H and D atoms during H_2-D_2 exchange over B2 and FCC $Pd_{47}Cu_{53}$ are plotted in Figure 6b. At low temperatures (~200 K), both the B2 and FCC $Pd_{47}Cu_{53}$ surfaces are nearly saturated with H and D atoms. As the temperature increases and desorption rate increases, the total coverage decreases on both surfaces. The coverage decreases more

dx.doi.org/10.1021/jp2076885 |J. Phys. Chem. C 2011, 115, 24221–24230

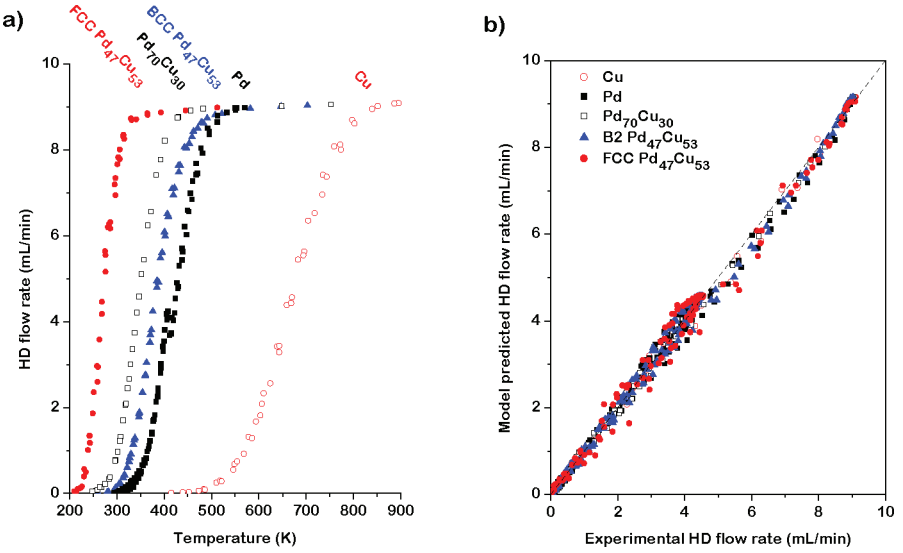

Figure 7. a) Comparison of the HD flow rates exiting Pd, Cu, $Pd_{70}Cu_{30}$, B2 $Pd_{47}Cu_{53}$, and FCC $Pd_{47}Cu_{53}$ foil catalyst beds, each with a catalyst surface area of ~19 cm^2 and 9 mL/min of H_2 and D_2 in the feed gas. (b) Parity plots illustrating the fits of the kinetic model for HD exchange (solid lines in Figures 2a, 4a, 5a, 6a) to the experimental data for HD exchange (discrete data points in Figures 2a, 4a, 5a, 6a).

rapidly on the FCC phase of $Pd_{47}Cu_{53}$ due to the smaller activation barrier to H_2 desorption on the FCC surface ($\Delta E_{des}^{\ddagger}$ = 0.46 ± 0.03 eV) than on the B2 surface ($\Delta E_{des}^{\ddagger}$ = 0.67 ± 0.03 eV).

Clearly, the crystal structure of $Pd_{47}Cu_{53}$ has a significant impact on the kinetics of H_2-D_2 exchange due to the differences in the energetics of H_2 adsorption and desorption on the two $Pd_{47}Cu_{53}$ phases. The activation barriers to H_2 adsorption on B2 $Pd_{47}Cu_{53}$ ($\Delta E_{ads}^{\ddagger}$ = 0.15 ± 0.02 eV) and on FCC $Pd_{47}Cu_{53}$ ($\Delta E_{ads}^{\ddagger}$ = 0.00 ± 0.02 eV) are not large, and H_2 adsorption rates on both surfaces were high. As a result, the rate of H_2-D_2 exchange over both the B2 and FCC $Pd_{47}Cu_{53}$ surfaces was influenced more by the rate of H_2 desorption than by the rate of adsorption.

The higher H_2-D_2 exchange activity exhibited by the FCC phase of $Pd_{47}Cu_{53}$ is due to a lower activation barrier to H_2 desorption on FCC $Pd_{47}Cu_{53}$ ($\Delta E_{des}^{\ddagger}$ = 0.46 ± 0.03 eV) than on B2 $Pd_{47}Cu_{53}$ ($\Delta E_{des}^{\ddagger}$ = 0.67 ± 0.03 eV). The fundamental reason(s) for this difference are unclear.

4.5. Comparison of H_2-D_2 Exchange over Pd, Cu, $Pd_{70}Cu_{30}$, and $Pd_{47}Cu_{53}$. A comparison of the HD flow rates exiting the Pd, Cu, $Pd_{70}Cu_{30}$, B2 $Pd_{47}Cu_{53}$, and FCC $Pd_{47}Cu_{53}$ catalyst beds, with 9 mL/min each of H_2 and D_2 in the feed gas, is shown in Figure 7a. The H_2-D_2 exchange activity of Cu is much lower than that of Pd, $Pd_{70}Cu_{30}$, and $Pd_{47}Cu_{53}$ (B2 and FCC), and the PdCu alloys are more active for H_2-D_2 exchange than Pd.

The differences in the H_2-D_2 exchange activities of the catalysts are due to the differences in the energetics of H_2 adsorption and desorption on these catalysts. These energies have been evaluated as parameters in a kinetic model (Appendix A) that has been fit to the data in Figures 2, 4, 5, and 6. The quality of these fits is illustrated by the parity plots for all 5 samples shown in Figure 7b. A comparison of the energetics of H_2 adsorption on β-Pd-hydride, α-Pd-hydride, Cu, $Pd_{70}Cu_{30}$, B2 $Pd_{47}Cu_{53}$, and FCC $Pd_{47}Cu_{53}$ is shown in Figure 8. Table 2 lists the parameters that describe H_2 adsorption and desorption (ν_{ads}, $\Delta E_{ads}^{\ddagger}$, ν_{des}, $\Delta E_{des}^{\ddagger}$, and ΔE_{ads}) on β-Pd-hydride, α-Pd-hydride, Cu, $Pd_{70}Cu_{30}$, B2 $Pd_{47}Cu_{53}$, and FCC $Pd_{47}Cu_{53}$.

Cu is the least active H_2-D_2 exchange catalyst examined in this study due to the large activation barrier to H_2 adsorption on Cu

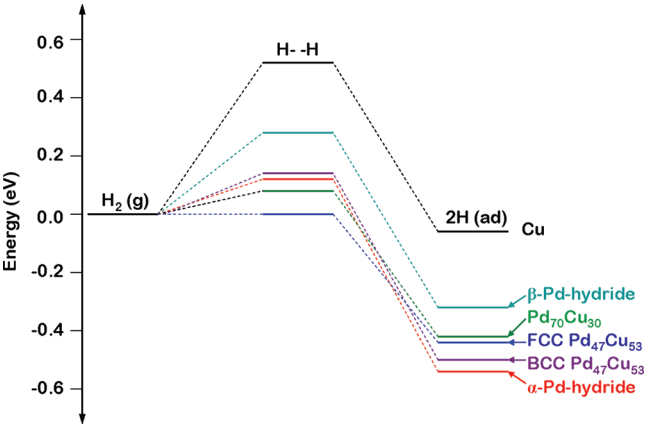

Figure 8. Potential energy diagram of H_2 adsorption on Cu, β-Pd-hydride, α-Pd-hydride, $Pd_{70}Cu_{30}$, B2 $Pd_{47}Cu_{53}$, and FCC $Pd_{47}Cu_{53}$.

($\Delta E_{ads}^{\ddagger}$ = 0.54 ± 0.06 eV). In contrast, barriers to H_2 adsorption on β-Pd-hydride ($\Delta E_{ads}^{\ddagger}$ = 0.3 ± 0.1 eV), α-Pd-hydride ($\Delta E_{ads}^{\ddagger}$ = 0.12 ± 0.04 eV), $Pd_{70}Cu_{30}$ ($\Delta E_{ads}^{\ddagger}$ = 0.09 ± 0.02 eV), B2 $Pd_{47}Cu_{53}$ ($\Delta E_{ads}^{\ddagger}$ = 0.15 ± 0.02 eV), and FCC $Pd_{47}Cu_{53}$ ($\Delta E_{ads}^{\ddagger}$ = 0.00 ± 0.02 eV) are relatively small, and the rate of H_2-D_2 exchange over these catalysts is determined largely by the rate of H_2 desorption (desorption-limited). FCC $Pd_{47}Cu_{53}$ has the highest H_2-D_2 exchange activity of the desorption-limited catalysts because the activation barrier to H_2 desorption on FCC $Pd_{47}Cu_{53}$ ($\Delta E_{des}^{\ddagger}$ = 0.46 ± 0.03 eV) is the smallest. As expected, the order of decreasing H_2-D_2 exchange activity of the desorption-limited catalysts (FCC $Pd_{47}Cu_{53}$ < $Pd_{70}Cu_{30}$ < B2 $Pd_{47}Cu_{53}$ < β-Pd-hydride < α-Pd-hydride) follows closely the order of increasing activation barrier to H_2 desorption: FCC $Pd_{47}Cu_{53}$ ($\Delta E_{des}^{\ddagger}$ = 0.46 ± 0.03 eV) < $Pd_{70}Cu_{30}$ ($\Delta E_{des}^{\ddagger}$ = 0.52 ± 0.02 eV) < β-Pd-hydride ($\Delta E_{des}^{\ddagger}$ = 0.63 ± 0.03 eV) < B2 $Pd_{47}Cu_{53}$ ($\Delta E_{des}^{\ddagger}$ = 0.67 ± 0.03 eV) < α-Pd-hydride ($\Delta E_{des}^{\ddagger}$ = 0.68 ± 0.06 eV).

dx.doi.org/10.1021/jp2076885 |J. Phys. Chem. C 2011, 115, 24221–24230

The H_2 adsorption energy of (ΔE_{ads}) on α-Pd-hydride is the lowest (most negative) of the catalysts, and therefore, H atoms are the most stable on α-Pd-hydride. The order of increasing heat of adsorption of H_2 (decreasing stability of H atoms) on the catalysts is as follows: α-Pd-hydride ($\Delta E_{ads} = -0.56 \pm 0.07$ eV) < B2 $Pd_{47}Cu_{53}$ ($\Delta E_{ads} = -0.52 \pm 0.04$ eV) < FCC $Pd_{47}Cu_{53}$ ($\Delta E_{ads} = -0.46 \pm 0.03$ eV) < $Pd_{70}Cu_{30}$ ($\Delta E_{ads} = -0.43 \pm 0.03$ eV) < β-Pd-hydride ($\Delta E_{ads} = -0.3 \pm 0.1$ eV) < Cu ($\Delta E_{ads} = 0.0 \pm 0.7$ eV). The heat of adsorption of H_2 on the PdCu alloys is not much greater (less negative) than that on α-Pd-hydride, indicating that alloying Pd with Cu does not drastically reduce the stability of H atom adsorption.

Experimental pre-exponents can be compared to values estimated by statistical mechanics methods. The pre-exponent for H_2 desorption (ν_{des}) is $\sim 10^6$ mol/m^2/s for all of the catalysts examined in this study. This value compares well with statistical mechanics estimates, which range from 10^6 to 10^8 mol/m^2/s, depending on assumptions about the mobility of the transition state.[48] For dissociative adsorption, experimental pre-exponents are on the order of 10^{-5} mol/m^2/s/Pa; statistical mechanics analysis predicts 10^{-2} to 10^{-4}, again depending on assumptions about transition state mobility.[48]

The results of this study are significant because it has been shown that (1) the crystal structures of Pd (β-Pd-hydride and α-Pd-hydride) and of $Pd_{47}Cu_{53}$ (B2 and FCC) have a significant impact on the energetics of H_2 adsorption and desorption and (2) although the H_2 dissociation activity of Cu is very low, Pd can be alloyed with as much as ~50 mol % Cu without significantly reducing H_2 dissociation rates.

5. CONCLUSIONS

The energetics of H_2 adsorption on Pd, Cu, $Pd_{70}Cu_{30}$, and $Pd_{47}Cu_{53}$ were investigated by microkinetic analysis of H_2-D_2 exchange data acquired over fixed beds of diced single-component and alloy foils. For both Pd phases (β-Pd-hydride and α-Pd-hydride) and both $Pd_{47}Cu_{53}$ phases (B2 and FCC) crystal structure had a significant impact on the kinetics of H_2-D_2 exchange. The H_2-D_2 exchange activity of FCC $Pd_{47}Cu_{53}$ was the highest of all the catalysts in this study and the H_2-D_2 exchange activity of the catalysts decreases in the following order: FCC $Pd_{47}Cu_{53}$ > $Pd_{70}Cu_{30}$ > B2 $Pd_{47}Cu_{53}$ > β-Pd-hydride > α-Pd-hydride ≫ Cu. The very low H_2-D_2 exchange activity of the Cu catalyst is due to the large activation barrier to H_2 adsorption on Cu ($\Delta E_{ads}^{\ddagger} = 0.54 \pm 0.06$ eV). Activation barriers to H_2 adsorption on β-Pd-hydride ($\Delta E_{ads}^{\ddagger} = 0.3 \pm 0.1$ eV), α-Pd-hydride ($\Delta E_{ads}^{\ddagger} = 0.12 \pm 0.04$ eV), $Pd_{70}Cu_{30}$ ($\Delta E_{ads}^{\ddagger} = 0.09 \pm 0.02$ eV), B2 $Pd_{47}Cu_{53}$ ($\Delta E_{ads}^{\ddagger} = 0.15 \pm 0.02$ eV), and FCC $Pd_{47}Cu_{53}$ ($\Delta E_{ads}^{\ddagger} = 0.00 \pm 0.02$ eV) are small relative to that for Cu and the rate of H_2-D_2 exchange over these catalysts was determined largely by the rate of H_2, D_2, and HD desorption (desorption-limited). The order of decreasing H_2-D_2 exchange activity in the desorption-limited catalysts is nearly the same as the order of increasing activation barrier for H_2 desorption: FCC $Pd_{47}Cu_{53}$ ($\Delta E_{des}^{\ddagger} = 0.46 \pm 0.03$ eV) < $Pd_{70}Cu_{30}$ ($\Delta E_{des}^{\ddagger} = 0.52 \pm 0.02$ eV) < β-Pd-hydride ($\Delta E_{des}^{\ddagger} = 0.63 \pm 0.03$ eV) < B2 $Pd_{47}Cu_{53}$ ($\Delta E_{des}^{\ddagger} = 0.67 \pm 0.03$ eV) < α-Pd-hydride ($\Delta E_{des}^{\ddagger} = 0.68 \pm 0.06$ eV). These results are significant for H_2 separation membrane applications because they demonstrate that Pd can be alloyed with as much as ~50 mol % Cu without significantly reducing its activity for dissociative H_2 adsorption.

APPENDIX: DERIVATION OF THE H_2-D_2 EXCHANGE KINETIC MODEL

The integral mass balance on HD is

$$\int_0^{F_{HD,out}} \frac{dF_{HD}}{r_{HD}} = A \tag{A1}$$

where dF_{HD} is the differential HD flow rate, $F_{HD,out}$ is the HD flow rate exiting the catalyst bed, A is the catalyst surface area, and r_{HD} is the HD production rate.[49] The HD production rate, r_{HD}, is given by the microkinetic expression

$$r_{HD} = 2k_{des}\theta_H\theta_D - k_{ads}P_{HD}(1-\theta_H-\theta_D)^2 \tag{A2}$$

where k_{des} is the HD desorption rate constant, θ_H is the coverage of H atoms, θ_D is the coverage of D atoms, k_{ads} is the HD adsorption rate constant, and P_{HD} is the HD partial pressure. Because we are assuming that isotopic effects are negligible and the partial pressures of H_2 and D_2 are equal for all experiments, the coverages of H (θ_H) and D (θ_H) atoms are each assumed to be equal to one-half of the total coverage (θ): $\theta_H = \theta_D = (\theta/2)$. Therefore, the microkinetic expression for the rate of HD production is

$$r_{HD} = 2k_{des}\left(\frac{\theta}{2}\right)^2 - k_{ads}P_{HD}(1-\theta)^2 \tag{A3}$$

To substitute the microkinetic expression for the rate of HD production, eq A3, into the mass balance on HD, eq A1, the HD partial pressure in eq A3 must be converted into HD flow rate, F_{HD}

$$r_{HD} = 2k_{des}\left(\frac{\theta}{2}\right)^2 - \frac{k_{ads}F_{HD}P_{total}(1-\theta)^2}{F_{total}} \tag{A4}$$

where

$$F_{HD} = \frac{F_{total}P_{HD}}{P_{total}}$$

and P_{total} is the total pressure and F_{total} is the total flow rate. Substituting the HD production rate, eq A4, into the integral mass balance on HD, eq A1, gives

$$\int_0^{F_{HD,out}} \frac{dF_{HD}}{2k_{ads}\left(\frac{\theta}{2}\right)^2 - \frac{k_{ads}F_{HD}P_{total}(1-\theta)^2}{F_{total}}} = A \tag{A5}$$

Integrating eq A5 and solving for the flow rate of HD exiting the catalyst bed gives

$$F_{HD,out} = \frac{k_{ads}F_{total}\theta^2}{2k_{ads}P(1-\theta)^2}\left[1 - \exp\left(-\frac{k_{ads}PA(1-\theta)^2}{F_{total}}\right)\right] \tag{A6}$$

At steady state, the change in the coverage of H (and D) atoms is zero

$$\frac{d\theta_H}{dt} = 0 = 2k_{ads}P_{H_2}(1-\theta_H-\theta_D)^2 + k_{ads}P_{HD}(1-\theta_H-\theta_D)^2 - 2k_{ads}\theta_H^2 - 2k_{ads}\theta_H\theta_D$$

where P_{H_2} is the H_2 partial pressure and all of the other variables are defined above. Again, we assume that the coverages of H and D atoms are each equal to one-half of the total

coverage: $\theta_H = \theta_D = (\theta/2)$. Therefore, the change in the coverage of H atoms is given by

$$\frac{d\theta_H}{dt} = 0 = 2k_{ads}P_{H2}(1-\theta)^2 + k_{ads}P_{HD}(1-\theta)^2 - k_{ads}\theta^2$$

Solving for θ gives

$$\theta = \frac{\sqrt{2\frac{k_{ads}}{k_{des}}P_{H_2,feed}}}{1+\sqrt{2\frac{k_{ads}}{k_{des}}P_{H_2,feed}}} \quad (A7)$$

where $P_{H_2,feed}$ is the partial pressure of H_2 in the feed gas, which is related to P_{H_2} and P_{HD} by the stoichiometry of the reaction

$$P_{H_2} = P_{H_2,feed} - \frac{1}{2}P_{HD}$$

Substitution of the expression for the total coverage of H and D atoms, eq A7, into the expression for the flow rate of HD exiting the reactor, eq A6, gives the H_2-D_2 exchange kinetic model

$$F_{HD,out} = F_{H_2,feed}\left[1-\exp\left(\frac{-k_{ads}p_{total}A}{F_{total}\left(1+\sqrt{2\frac{k_{ads}}{k_{des}}P_{H_2,feed}}\right)^2}\right)\right] \quad (A8)$$

where

$$F_{H_2,feed} = \frac{F_{total}P_{H_2,feed}}{p_{total}}$$

AUTHOR INFORMATION

Corresponding Author

*E-mail: gellman@andrew.cmu.edu. Phone: (412) 268-3848.

REFERENCES

(1) Howard, B. H.; Killmeyer, R. P.; Rothenberger, K. S.; Cugini, A. V.; Morreale, B. D.; Enick, R. M.; Bustamante, F. *J. Membr. Sci.* **2004**, *241*, 207.

(2) Steward, S. A. *Review of Hydrogen Isotope Permeability through Materials*; Lawrence Livermore National Laboratory: 1983; pp 1−21.

(3) Lewis, F. A. *The Palladium-Hydrogen System*; Academic Press: New York, 1967.

(4) Peisl, H. *Hydrogen in Metals I*; Springer-Verlag: Berlin, 1978; Vol. 28.

(5) Kamakoti, P.; Morreale, B. D.; Ciocco, M. V.; Howard, B. H.; Killmeyer, R. P.; Cugini, A. V.; Sholl, D. S. *Science* **2005**, *307*, 569.

(6) Kulprathipanja, A.; Alptekin, G. O.; Falconer, J. L.; Way, J. D. *J. Membr. Sci.* **2005**, *254*, 49.

(7) Morreale, B. D. *The Influence of H_2S on Palladium and Palladium-Copper Alloy Membranes*; University of Pittsburgh; Pittsburgh, PA, 2006.

(8) Morreale, B. D.; Howard, B. H.; Iyoha, O.; Enick, R. M.; Ling, C.; Sholl, D. S. *Ind. Eng. Chem. Res.* **2007**, *46*, 6313.

(9) O'Brien, C. P.; Howard, B. H.; Miller, J. B.; Morreale, B. D.; Gellman, A. J. *J. Membr. Sci.* **2010**, *349* (1−2), 380.

(10) Chen, C. H.; Ma, Y. H. *J. Membr. Sci.* **2010**, *362*, 535.

(11) Pan, X.; Kilgus, M.; Goldbach, A. *Catal. Today* **2005**, *104*, 225.

(12) Morreale, B. D.; Ciocco, M. V.; Howard, B. H.; Killmeyer, R. P.; Cugini, A. V.; Enick, R. M. *J. Membr. Sci.* **2004**, *241*, 219.

(13) Yang, J. Y.; Nishimura, C.; Komaki, M. *J. Alloys Compd.* **2007**, 446.

(14) Yang, J. Y.; Nishimura, C.; Komaki, M. *J. Membr. Sci.* **2008**, *309*, 246.

(15) Iyoha, O.; Enick, R.; Killmeyer, R.; Morreale, B. *J. Membr. Sci.* **2007**, *305*, 77.

(16) Iyoha, O.; Enick, R. R.; Killmeyer, R. P.; Howard, B.; Ciocco, M.; Morreale, B. *J. Membr. Sci.* **2007**, *306*, 103.

(17) Muschiol, U.; Schmidt, P. K.; Christman, K. *Surf. Sci.* **1998**, *395*, 182.

(18) Cattania, M. G.; Penka, V.; Behm, R. J.; Christmann, K.; Ertl, G. *Surf. Sci.* **1983**, *126*, 382–391.

(19) Lozano, A.; Gross, A.; Busnengo, H. F. *Phys. Rev. B* **2010**, *81*, 121402(R).

(20) Bartczak, W. M.; Stawowska, J. *Struct. Chem.* **2004**, *15*, 447.

(21) Dong, W.; Kresse, G.; Hafner, J. *J. Mol. Catal A: Chem.* **1997**, *119*, 69.

(22) Wang, Z. S.; Darling, G. R.; Holloway, S. *J. Chem. Phys.* **2004**, *120*, 2923.

(23) Hammer, B.; Scheffler, M.; Jacobsen, K. W.; Norskov, J. K. *Phys. Rev. Lett.* **1994**, *73*, 1400.

(24) Rettner, C. T.; Michelsen, H. A.; Auerbach, D. J. *J. Chem. Phys.* **1995**, *102*, 4625.

(25) Murphy, M. J.; Hodgson, A. *J. Chem. Phys.* **1998**, *108*, 4199.

(26) Abbott, H. L.; Harrison, I. *J. Phys. Chem. A* **2007**, *111*, 9871.

(27) Campbell, J. M.; Campbell, C. T. *Surf. Sci.* **1991**, *259*, 1.

(28) Rasmussen, P. B.; Holmblad, P. M.; Christoffersen, H.; Taylor, P. A.; Chorkendorff, I. *Surf. Sci.* **1994**, *287/288*, 79.

(29) Hayden, B. E.; Lamont, C. L. A. *Surf. Sci.* **1991**, *243*, 31.

(30) Sakong, S.; Axel, G. *Surf. Sci.* **2003**, *525*, 107.

(31) Hammer, B. *Surf. Sci.* **1995**, *343*, 211.

(32) Sun, Q.; Xie, J.; Tao, Z. *Surf. Sci.* **1995**, *338*, 11.

(33) Yuan, L. *J. Phys. Chem. B* **2007**, *111*, 10952.

(34) McQuarrie, D. A. *Statistical Mechanics*; University Science Books: 2000.

(35) Levie, R. D. *J. Chem. Educ.* **1999**, *76*, 1594.

(36) Johansson, M.; Skulason, E.; Nielsen, G.; Murphy, S.; Nielsen, R. M.; Chorkendorff, I. *Surf. Sci.* **2010**, *604*, 718.

(37) Jewell, L. L. *Appl. Catal, A* **2006**, *310*, 1.

(38) Switendick, A. C. *Hydrogen in Metals I*; Springer-Verlag: Berlin, 1978.

(39) Flanagan, T. B. *Annu. Rev. Mater. Sci.* **1991**, 269.

(40) Roudgar, A.; Gross, A. *Surf. Sci.* **2005**, *597*, 42.

(41) Sykes, E. C.; Fernandez-Torres, L. C.; Nanayakkara, S. U.; Mantooth, B. A.; Nevin, R. M.; Weiss, P. S. *Proc. Natl. Acad. Sci. U.S.A.* **2005**, *102*, 17907.

(42) Johansson, M.; Lytken, O.; Chorkendorff, I. The sticking probability of hydrogen on Ni, Pd and Pt at a hydrogen pressure of 1 bar. *Top. Catal.* **2007**, *46*, 175–187.

(43) Okuyama, H.; Siga, W.; Takagi, N.; Nishijima, M.; Aruga, T. *Surf. Sci.* **1998**, *401*, 344.

(44) Johansson, M.; Lytken, O.; Chorkendorff, I. *Surf. Sci.* **2008**, *602*, 1863.

(45) Wilke, S. *Phys. Rev. Lett.* **1996**, *76*, 4.

(46) Wilke, S. *Surf. Sci.* **1995**, *329*, L605.

(47) Gravil, P. A. *Surf. Sci.* **1999**, *430*, 176.

(48) Dumesic, J. A.; Rudd, D. F.; Apraicio, L. M.; Rekoske, J. E.; Trevino, A. A. The Microkinetics of Heterogeneous Catalysis. In American Chemical Society: Washington DC, 1993; p 40.

(49) Fogler, H. S. *Elements of Chemical Reaction Engineering*. Prentice-Hall International, Inc.: 1999.